

Punching failure – influence of material properties and size effect

J.Ožbolt, H.Vocke & R.Eligehausen

Institute of Construction Materials, University of Stuttgart, Germany

ABSTRACT: In the present paper the results of a three-dimensional finite element analysis of punching failure in reinforced concrete slabs are presented and discussed. The analysis is carried out using the three-dimensional special purpose finite-element code *MASA*. To demonstrate that the code is able to realistically predict punching failure, a punching test on an interior slab-column connection is simulated and the results are compared with the test results. Subsequently, a parametric study is performed where the concrete properties and the reinforcement ratio are varied. To investigate the size effect, for a fixed set of material parameters the slab geometry is scaled. The results of the study are discussed and compared with design code recommendations.

1 INTRODUCTION

A finite-element analysis based on a realistic material model for concrete is a helpful tool for the development of analytical models for punching failure of reinforced concrete flat slabs. It serves as a support of the experimental studies in which several difficulties can appear. These are summarized as follows: (1) The available punching tests exhibit an enormous scatter with respect to test setups and test results, (2) within comparable test programs only a few parameters can be varied, (3) the tested slab thickness and column dimensions are relatively small (size effect), (4) important material properties of concrete, such as fracture energy and tensile strength, can not directly be controlled, (5) the formation and propagation of internal cracks can not directly be observed during the test and (6) punching tests are rather expensive.

In numerous investigations it has been shown that in the present paper employed finite element code is able to realistically predict the behaviour of reinforced concrete structures (Ožbolt et al. 1999). In the present study a brief overview of the program is given. Subsequently, the results of a numerical simulation of a punching test are presented and compared with the experimental results. Finally, a parametric study is carried out in which the influence of material and geometrical properties on the punching behaviour is studied. The results are discussed and compared with design code recommendations.

2 FINITE-ELEMENT-CODE *MASA*

2.1 *General*

The FE-code *MASA* (Ožbolt 1998) is aimed to be used for the two- and three-dimensional linear and non-linear analysis of structures made of quasi-brittle materials such as concrete. The program is based on the microplane material model (Ožbolt et al. 2001) and a smeared crack approach. To avoid a spurious mesh sensitivity either the improved crack band approach (stress relaxation method) (Bažant & Oh 1983, Ožbolt 1999) or the nonlocal integral approach (Ožbolt & Bažant 1996, Pijaudier-Cabot & Bažant 1987) can be employed. The spatial discretization of concrete is performed by the four to eight node solid finite elements. The reinforcement can be modeled by discrete bar elements or, alternatively, smeared within the concrete elements. Moreover, particular contact elements (friction or spring elements) are available as well. The analysis is carried out incrementally, i.e. the load or displacement is applied in several steps. The preparation of the input data (nodes, elements, boundaries and loads) and the evaluation of the numerical results (element strains and stresses, nodal forces and displacements) are carried out with the commercial pre- and postprocessor *FEMAP*[®].

2.2 Microplane model and localization limiter

In the microplane model the material properties are characterized separately on planes of various orientations within the material. On these microplanes there are only a few uniaxial stress and strain components and no tensorial invariance requirements need to be considered. The tensorial invariance restrictions are satisfied automatically since the microplanes to some extent directly simulate the response on various weak planes in the material (inter-particle contact planes, interfaces, planes of microcracks, etc.). The constitutive properties are entirely characterized by relations between the stress and strain components on each microplane in both, normal and shear directions (Fig. 1). It is assumed that the strain components on the microplanes are projections of the macroscopic strain tensor (kinematic constraint approach). Knowing the stress-strain relationship of all microplane components, the macroscopic stiffness and the stress tensor are calculated from the actual strains on the microplanes by integrating the stress components on the microplanes over all directions. This integration is carried out numerically based on the method of virtual work. The simplicity of the model is due to the fact that only uniaxial stress-strain relationships are required for each microplane component and the macroscopic response is obtained automatically by integration over the microplanes. More details related to the used model can be found in Ožbolt et al. (2001).

The classical local continuum smeared fracture analysis of materials which exhibit softening (quasi-brittle materials) leads in the finite element analysis to results which are in general mesh dependent (Bažant & Oh 1983, Ožbolt 1999, Ožbolt & Bažant 1996, Pijaudier-Cabot & Bažant 1987). As well known, the reason for this is the localization of damage in finite elements and the related energy consumption capacity, which depends on the element size, i.e. if the finite element mesh is coarse the energy consumption capacity will be larger than if the mesh is fine. Consequently, the model response is mesh dependent. To assure mesh independent results the total energy consumption capacity due to cracking must be independent of the element size, i.e. one has to regularize the problem by introducing a so-called localization limiter. In the present numerical studies the crack band approach (Bažant & Oh 1983) is used in which the constitutive law is related to the element size. The basic assumption is that the damage localizes in a row of elements. Consequently, the constitutive law for each element is modified such that the area under the uniaxial compressive and tensile stress-strain relationship multiplied by the average element size approximately corresponds to the concrete compressive and tensile fracture energy, respectively.

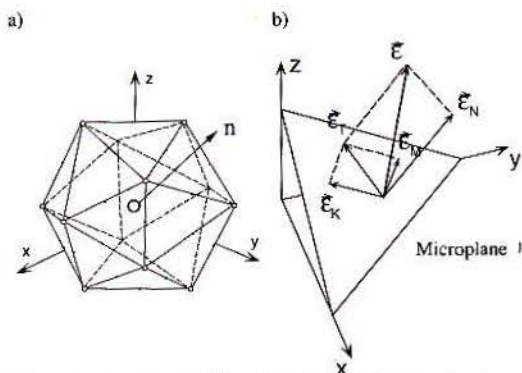


Figure 1. The concept of the microplane model: a) unit volume sphere - integration point and b) strain components.

3 VERIFICATION OF THE FE CODE

To demonstrate that the employed finite element code is able to realistically predict punching failure of reinforced concrete flat slabs, numerous punching tests from the literature have been simulated (Ožbolt et al. 1999). In the following, the results of the numerical simulation of a punching test from Hegger & Beutel (1998) are presented and the results are compared with the test results.

3.1 Geometry, spatial discretization and material properties

The geometry of the slab is shown in Figure 2a. The hexagonal specimen was vertically supported by 12 tie rods and loaded in the column with a hydraulic jack. The material properties and the arrangement of the reinforcement are summarized in Table 1. The reinforcement ratio was chosen as $\rho_1 = 0,8\%$. The slab was provided with no shear reinforcement. The finite-element mesh used in the simulation is shown in Figure 2b. For reasons of symmetry only a quarter of the test slab was modeled. In the region of punching the model was optimized by local mesh refinement. The spatial discretization of concrete was performed by 8-node solid elements. The reinforcing steel was modeled by 2-node bar elements, which were connected with the concrete elements via common nodes. The steel was represented by uniaxial ideally elasto-plastic stress-strain relationship. The load was applied by controlling the vertical displacement of the nodes at the bottom of the column area. To account for the confining effect of the column, these nodes were fixed in the horizontal directions. The support points were taken the same as in the experiment. To prevent local damage, the finite elements around the supporting nodes were defined as linear-elastic.

Table 1. Material properties of the test slab.

Concrete			Tensile Reinforcement			Compr. Reinforcement			
f_c	f_t	E	G_F	f_y	Number	ρ_t	f_y	Number	ρ_t
[MPa]	[MPa]	[MPa]	[N/mm]	[MPa]	[-]	[%]	[MPa]	[-]	[%]
21,0	1,73	21697	$\approx 0,10$	569	$\varnothing 14/10$	0,8	569	$\varnothing 10/175$	0,24

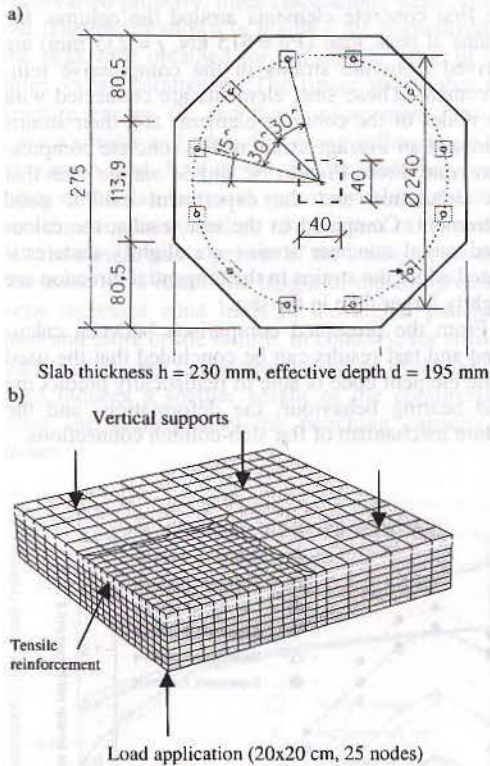


Figure 2. Punching of a flat slab: a) dimensions of test specimen, b) FE-mesh.

3.2 Numerical results and comparison with test results

The same as in the experiment, the failure obtained in the analysis is due to punching shear with the formation of the characteristic punching cone. Figure 3a shows the crack pattern in the post-peak regime. The cracks are plotted in terms of maximal principal strains (dark zones). The comparison with the corresponding test result (Fig. 3b) shows that the numerical simulation predicts the same shape of the punching cone as observed in the experiment.

The calculated and the experimentally measured load-deflection curves are plotted in Figure 4. The load corresponds to the vertical column force and the deflection is monitored on the column loading surface.

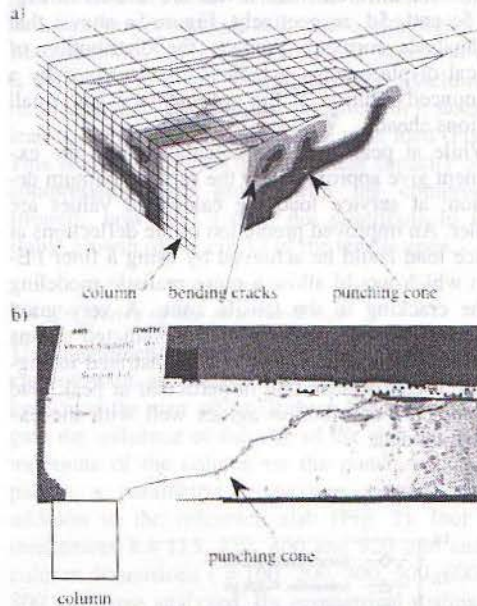


Figure 3. Crack pattern in the post-peak regime: a) simulation, in terms of maximum principal strains (dark zones), b) experiment.

As can be seen in Figure 4 the agreement between the numerical and measured data is reasonably good, the peak load and the corresponding displacement are very well estimated. However, the analysis exhibits a more ductile behavior in the post-peak regime. This is probably due to numerical reasons (convergence difficulties in the post-peak regime) and to the fact that the experiment was carried out load-controlled.

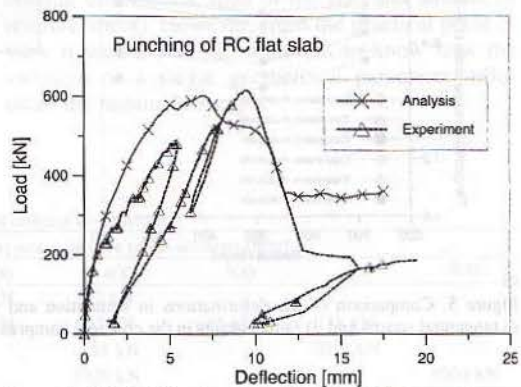


Figure 4. Calculated and measured load-deflection curves.

In Figure 5a the calculated and measured vertical deflections of the slab tensile surface are plotted for different load levels. Furthermore, Figure 5b shows the calculated and measured strains in the tensile reinforcement. The tangential strains and the radial strains in the concrete compression zone around the column for different load levels are shown in Figures 5c and 5d, respectively. Figure 5a shows that the analysis correctly predicts the distribution of vertical displacements, which is characterized by a pronounced rotation at the column face and small rotations ahead.

While at peak load the calculation and the experiment give approximately the same maximum deflection, at service load the calculated values are smaller. An improved prediction of the deflections at service load could be achieved by using a finer FE-mesh which would allow a more realistic modeling of the cracking in the tensile zone. A very good agreement between measured and predicted strains in the tensile reinforcement is demonstrated in Figure 5b. It can be seen that in particular at peak load the predicted distribution agrees well with the experimental data.

As mentioned above, the relatively low calculated strains at the level of the service load correspond to the small calculated deflections at this level (Fig. 5a). The tangential and radial strains in the concrete compression zone are shown in Figures 5c and 5d. To avoid a distortion of the calculated results due to an excessive localization of the strains in the first concrete elements around the column, the strains at peak load ($P_U = 615 \text{ kN}$, $r = 235 \text{ mm}$) are derived from the strains in the compressive reinforcement. These steel elements are connected with the nodes of the concrete elements and their strains represent an average strain of the concrete compression zone. From Figures 5c and 5d can be seen that the simulation and the experiment exhibit good agreement. Compared to the test results, the calculated radial concrete strains are slightly underestimated while the strains in the tangential direction are slightly larger than in the test.

From the presented comparison between calculated and test results can be concluded that the used finite element code is able to realistically predict the load bearing behaviour, the deformations and the failure mechanism of flat slab-column connections.

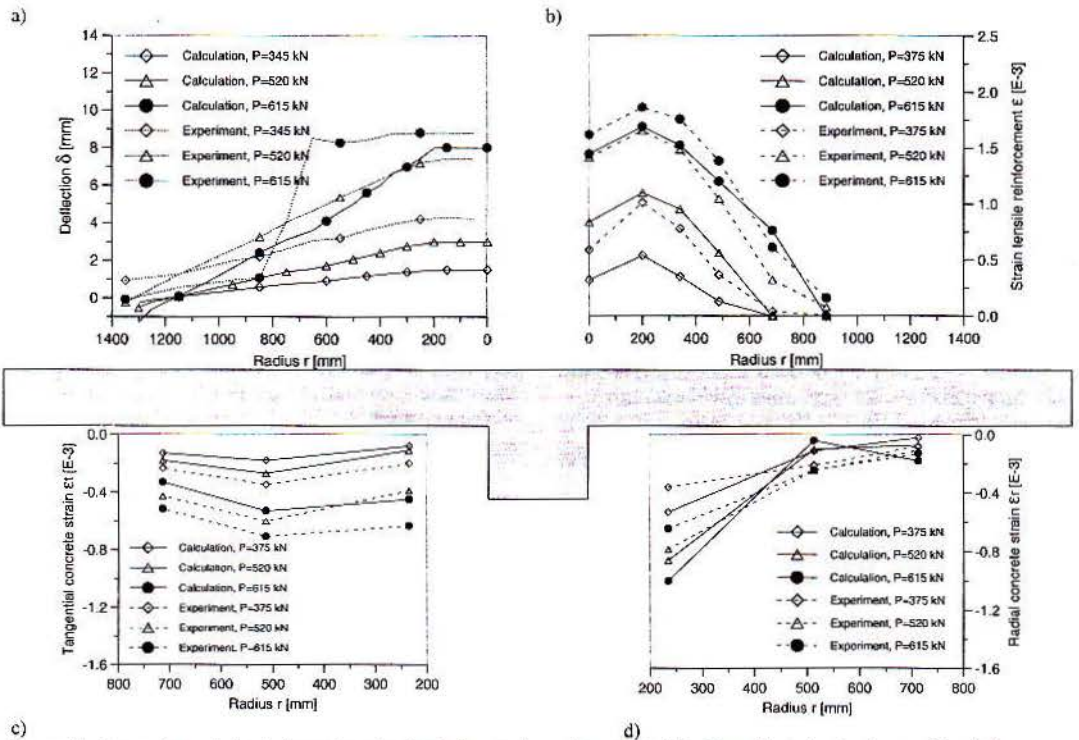


Figure 5. Comparison of the deformations in simulation and experiment: a) deflections, b) strains in the tensile reinforcement, c) tangential strains and d) radial strains in the concrete compression zone.

3.3 Influence of material parameters and reinforcement

The influence of the uniaxial cylinder compressive strength f_c , the concrete tensile strength f_t , the fracture energy G_F and the reinforcement ratio ρ_l on the punching capacity is summarized in Figure 6. For each varied property, three calculations were carried out. The results shown in Figure 6 are normalized to the peak load obtained for the middle value of the three varied parameters. The figure shows that the fracture energy G_F and the reinforcement ratio ρ_l have a similar and relatively strong influence on the maximum load. It is shown that the punching resistance of the slab increases approximately as the cube root function of G_F and ρ_l . High values of G_F and ρ_l lead to a more stable growth of the cracks in the tensile cord. As a result, the height of the compression zone increases what leads to the higher punching load and more brittle failure. In contrary, for smaller values of G_F and ρ_l the strong damage of the tensile cord induces a smaller height of the compression zone and consequently the punching capacity is lower.

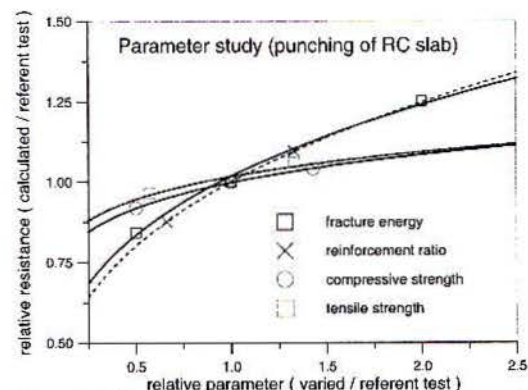


Figure 6. Influence of material properties and reinforcement ratio on the punching load.

Contrary to the influence of the fracture energy G_F and the reinforcement ratio ρ_l , the numerical results indicate a relatively small effect of the compressive and tensile concrete strength on the punching capacity (Fig. 6). A high tensile strength f_t does not lead to

a more stable propagation of shear cracks in the concrete which is of major importance for the punching response. Depending on the fracture energy G_F , the crack propagation at peak load might even become less stable if the tensile strength increases. Therefore, the positive effect of the tensile strength remains relatively small while the brittleness of the structural response tends to increase with higher tensile strengths. Provided that the reinforcement ratio is sufficient to avoid a flexural failure (yielding of reinforcement), the compressive strength f_c does not lead to significant increase of the peak load (Fig. 6). This is due to the fact that the shear capacity of the compression zone grows with the compressive strength, however, it does not contribute to more stable growth of the cracks of the tensile zone.

3.4 Influence of the structural size

The phenomenon that the nominal strength σ_N decreases with an increase of the structural size is known as the size effect (Bažant 1984). To investigate the influence of the size of the slab and the dimensions of the column on the punching load capacity, a parametric study was carried out. In addition to the reference slab (Fig. 2), four slab thicknesses $h = 115, 230, 460$ and 920 mm and six column dimensions $c = 100, 200, 300, 500, 600$ and 800 mm were analyzed. By geometrical scaling, the span of the slab and the amount of reinforcement were related to the thickness of the slab. For $h = 115, 460$ and 920 mm additional finite element meshes were generated. In all cases the concrete properties and the reinforcement ratio were kept constant and the same as specified in Table 1.

The calculated peak loads for all varied geometrical parameters are summarized in Table 2. These results can be evaluated from different points of view. Under size effect one generally considers the change of the nominal strength with an proportional increase of all structural dimensions (thickness of the slab, column dimensions, span of the slab and amount of reinforcement). However, from the practical point of view it would also be important to know how the variation of a single geometrical parameter influences the nominal strength.

Table 2. Calculated punching loads for different slab thicknesses and column dimensions.

h [mm]	d [mm]	column size c (square cross-section) [mm]						
		100	200	300	400	500	600	800
115	90	110 kN	150 kN	183 kN	212 kN	-	-	-
230	205	-	475 kN	568 kN	652 kN	688 kN	728 kN	-
460	435	-	-	-	1788 kN	-	2018 kN	-
920	860	-	-	-	3908 kN	-	-	5004 kN

3.4.1 Influence of the effective depth

For the proportional scaling of the slab and column geometry, in Figure 7 the nominal strength $\sigma_N = P_U/d(4c + \pi \cdot 3d)$ is plotted as a function of the effective depth of the slab. The calculated results are fitted by the Bazant (1984) size effect formula:

$$\sigma_N = B \cdot f_c \cdot (1 + d/d_0)^{-1/2} \quad (1)$$

where B and d_0 (characteristic size) are material and geometry dependent constants. They were obtained from a regression analysis of the calculated data ($B = 0.735$; $d_0 = 174$ mm). The nominal strength plotted in Figure 7 is scaled with a value of σ_N for $d = 205$ mm and with a constant $B \cdot f_c$.

The size effect curves according to Eurocode 2 and according to DIN 1045-1 are plotted as well. For the investigated size range the calculated data exhibits a relatively strong size effect on the nominal strength. The data are well fitted by the Bazant's type of the size effect formula. The relatively strong size effect could be expected since the parametric study indicated a strong sensitivity of the nominal strength on the variation of the fracture energy of concrete. The comparison with both design formulas, which are based on experimental results, shows relatively good agreement with the calculated data. For smaller sizes ($d < 200$ mm) both Eurocode 2 and DIN 1045-1 are conservative while for thick slabs ($d > 600$ mm) they are unsafe.

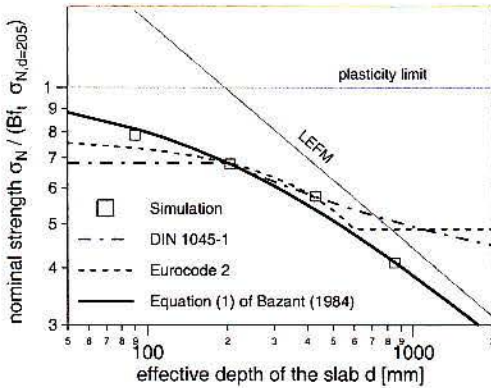


Figure 7. Size effect on the nominal strength - proportional scaling of the slab and column geometry.

Figure 8 shows calculated crack patterns at peak load for slabs $h = 230$ mm and $h = 920$ mm. As can be seen, the relative length of the diagonal shear crack for both slab sizes is approximately the same. This confirms proportionality of the crack length at peak load, i.e. the stable crack growth takes place and the main assumption of the Bazant's size effect formula is fulfilled.

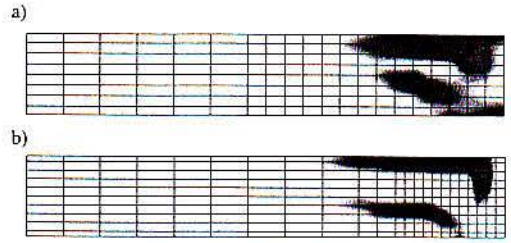


Figure 8. Calculated crack pattern at peak load (maximal principal strains for crack width of 0.15 mm): a) $h = 230$ mm and b) $h = 920$ mm.

3.4.2 Influence of the column dimensions

Punching failure is characterized by a concentrated state of radial and tangential compressive strains in the concrete around the column. The intensity of this state of strains is essential for the punching capacity and depends also on the column dimensions. With increasing the dimensions of the column the intensity especially of the tangential concrete strains will decrease. As a result, it can be expected that the nominal shear strength σ_N will decrease with larger column dimensions. Theoretically, there is a transition of the nominal shear strength σ_N from very high values for very small columns (punctual load application) to the level of line-supported slabs for very large column dimensions.

In Figure 9 the nominal shear strength σ_N of the slab is plotted as a function of the column size c . The results are shown for two effective depths, $d = 90$ and $d = 205$ mm. For both slabs the shear span ratio a/d was constant.

In Figure 9a the nominal shear strength is calculated according to DIN 1045 as $\sigma_N = P_U/d \cdot \pi \cdot (1,13 \cdot c + d)$, i.e. it is assumed that the critical cross-section is placed at a distance $d/2$ from the column face. In contrary to the design formula, the numerical results show that for both slab thickness the nominal shear strength decreases with an increase of the column size. For very large columns, the nominal shear strength tends towards the nominal shear strength of line-supported slabs. This transition of the shear strength is due to the fact that the intensity of the compressive strains in the vicinity of the column which governs the shear strength of the slab decreases with increasing the column size. Furthermore, the comparison with DIN 1045 shows that the numerical results agree well with the design code recommendations for slabs with small columns while for large columns the design code recommendations of DIN 1045 become unsafe.

In Figure 9b the nominal shear strength is calculated according to Eurocode 2 with $\sigma_N = P_U/d \cdot (4c + \pi \cdot 3d)$. The critical cross-section is assumed to be placed at distance $1.5d$ from the column surface. Based on this critical section the numerical results show for both slab thickness that the nominal shear strength is not much influenced by the

column size. For $d = 90$ mm the results are in very good agreement with EC2 design code recommendations. However, for $d = 205$ mm the code slightly underestimates the predicted numerical results.

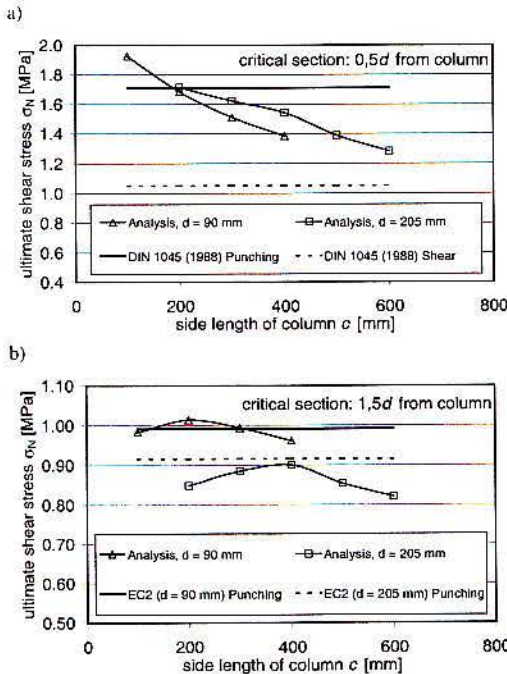


Figure 9. Nominal shear stress σ_N in a critical section u_{crit} according to: a) DIN 1045, b) Eurocode 2

4 CONCLUSIONS

Based on the results presented in the paper the following conclusions can be drawn: (1) The three-dimensional finite-element code used in the present study is based on the microplane material model for concrete and a smeared crack approach. The comparison between experimental results and results of the numerical simulation demonstrate that the code is able to realistically predict the load-bearing and deformation behaviour as well as the failure mode of slab-column connections; (2) The numerical analysis shows that for the investigated slab geometry the fracture energy and the reinforcement ratio give a dominant influence on the punching capacity which increases approximately proportionally to the cube root of these parameters. In contrary, the influence of the concrete compressive and tensile strength is relatively small. The structural response becomes more brittle when the values of the varied parameters increase; (3) The results of the parametric study confirm that the maximum load and the fracture

mechanism of reinforced concrete structures which exhibit complex cracking (i.e. no fracture upon first formation of a crack) do not primarily depend on the tensile strength of the concrete but on the entire tensile behaviour which is characterized by the interaction of tensile strength and fracture energy; (4) Finally, it is demonstrated that increasing the effective depth d leads to a decrease of the nominal shear capacity of the slabs. For the investigated size range the numerical prediction shows good agreement with the design code recommendations.

5 REFERENCES

- Bažant, Z.P. & Oh, B.-H. 1983. Crack Band Theory for Fracture of Concrete. *Materials and Structures* 93(16): 155-177.
- Bažant, Z.P. 1984. Size Effect in Blunt Fracture: Concrete, Rock, Metal. *Journal of Engineering Mechanics* 110(4): 518-535.
- DIN 1045 1988. Beton und Stahlbeton; Bemessung und Ausführung. *German Standard*.
- DIN 1045-1 2000. Tragwerke aus Beton, Stahlbeton und Spannbeton; Teil 1: Bemessung und Konstruktion. *German Standard (Draft)*.
- Eurocode 2 1991. Design of concrete structures. *European Prestandard*.
- FEMAP – Finite Element Modeling and Postprocessing, Ver. 5.00a, Copyright © 1985-1997, Enterprise Software Products Inc.
- Hegger, J. & Beutel, R. 1998. Durchstanzen schubbewehrter Flachdecken im Bereich von Innenstützen. *Final Report AiF-Forschungsvorhaben 10644N, Lehrstuhl und Institut für Massivbau, RWTH Aachen*.
- Ožbolt, J. & Bažant, Z.P. 1996. Numerical smeared fracture analysis: Nonlocal microcrack interaction approach. *International Journal for Numerical Methods in Engineering*, 39(4): 635-661.
- Ožbolt, J. & Vocke, H. 1999. Numerische Untersuchungen zum Durchstanzen von Flachdecken. *Report in preparation, Institut für Werkstoffe im Bauwesen, Universität Stuttgart*.
- Ožbolt, J., Li, Y.-J. and Kožar, I. 2001. Microplane model for concrete with relaxed kinematic constraint. *International Journal of Solids and Structures*, in press.
- Ožbolt, J. 1998. MASA – MACROscopic Space Analysis. *Report for the description of MASA, Institut für Werkstoffe im Bauwesen, Universität Stuttgart*.
- Ožbolt, J. 1999. Nonlocal fracture analysis - stress relaxation method. *Report, Institut für Werkstoffe im Bauwesen, Universität Stuttgart*.
- Ožbolt, J.; Mayer, U.; Vocke, H. & Eligehausen, R. 1999. Verschmierte Rissmethode. *Beton- und Stahlbetonbau*, 94 (10), 403-412.
- Pijaudier-Cabot, G. & Bažant, Z.P. 1987. Nonlocal Damage Theory. *Journal of Engineering Mechanics*, 113(10): 1512-1533.